Characterization of thylakoid lipid membranes from cyanobacteria and higher plants by molecular dynamics simulations

CrossMark

Floris J. van Eerden [a],*, Djurre H. de Jong [b], Alex H. de Vries [a], Tsjerk A. Wassenaar [c], Siewert J. Marrink [a]

[a] Groningen Biomolecular Sciences and Biotechnology Institute and Zernike Institute for Advanced Materials, University of Groningen, Nijenborgh 7, 9747 AG Groningen, The Netherlands
[b] Institut für Physikalische Chemie, Westfälische Wilhelms-Universität Münster, 48149 Münster, Germany
[c] Computational Biology, Department of Biology, University of Erlangen-Nürnberg, Staudtstr. 5, 91052 Erlangen Germany

ABSTRACT

The thylakoid membrane is mainly composed of non-common lipids, so called galactolipids. Despite the importance of these lipids for the function of the photosynthetic reaction centers, the molecular organization of these membranes is largely unexplored. Here we use multiscale molecular dynamics simulations to characterize the thylakoid membrane of both cyanobacteria and higher plants. We consider mixtures of up to five different galactolipids plus phosphatidylglycerol to represent these complex membranes. We find that the different lipids generally mix well, although nanoscale heterogeneities are observed especially in case of the plant membrane. The fluidity of the cyanobacterial membrane is markedly reduced compared to the plant membrane, even considering elevated temperatures at which thermophilic cyanobacteria are found. We also find that the plant membrane more readily undergoes a phase transformation to an inverted hexagonal phase. We furthermore characterized the conformation and dynamics of the cofactors plastoquinone and plastoquinol, revealing of the fast flip-flop rates for the non-reduced form. Together, our results provide a molecular view on the dynamical organization of the thylakoid membrane.

© 2015 Elsevier B.V. All rights reserved.

1. Introduction

The thylakoid membrane is essential for most forms of life. It has the special capability to perform photosynthesis, the process in which solar energy is harvested and converted into biochemical energy. The thylakoid membrane is located inside chloroplasts and in the lumen of cyanobacteria. Only the light-dependent reactions of photosynthesis, in which ATP and NADPH are generated, take place in the thylakoid membrane. Photosynthesis is the result of a complex interplay between the proteins embedded in the thylakoid membrane, the lipids that make up the thylakoid membrane and a set of cofactors [1,2]. The most important photosynthetic proteins are photosystem II (PSII) and photosystem I (PSI) with the associated light-harvesting complexes (LHC), the cytochrome b_6/f complex and ATP synthase.

Four unique lipid classes make up the thylakoid membrane: phosphatidylglycerol (PG) (~13%), digalactosyldiacylglycerol (DGDG) (~32%), monogalactosyldiacylglycerol (MGDG) (~40%) and sulfoquinovosyldiacylglycerol (SQDG) (~15%) [2,3]. This composition is highly conserved in oxygenic organisms, but the type and stoichiometry of the lipid tails vary per species [2,4]. A growing number of studies indicate that the special lipid composition of the thylakoid membrane is mandatory for the proper functioning of the photosynthetic machinery [5].

In vivo the thylakoid lipids are organized as bilayers [6,7], but the overall composition gives the thylakoid membrane a high propensity to form non-bilayer phases [6]. Indeed a total lipid extract from the chloroplast membrane does not form bilayers in water [8]. PG, SQDG and DGDG are all bilayer forming lipids, but the most prominent component of the thylakoid membrane, MGDG, forms inverted hexagonal phases [9, 10]. Next to the lamellar phase, a non-lamellar lipid phase of the thylakoid membrane might be required for photosynthesis [11]. It has been proposed that inverted hexagonal phases are important for the violaxanthin cycle, by facilitating the flip-flop of antheraxin. It is assumed that these inverted hexagonal phases are preferentially located in MGDG rich domains and that violaxanthin de-expoxidase especially binds in MGDG rich domains [12–14]. In the literature there is some uncertainty about the lateral heterogeneity in the thylakoid membrane. Initially it was thought that the various regions of the thylakoid membrane have different lipid compositions [15], but more recently it was shown that the bulk lipids of the thylakoid membrane do not display lateral heterogeneity [16]. The resolution of these techniques is, however, on a mesoscopic scale, and a detailed view of the nanoscale organization of thylakoid membranes is currently lacking.

In order to provide such a view and to obtain a more fundamental level understanding of the role of lipids in the thylakoid membrane,

* Corresponding author at: Nijenborgh 7, 9747 AG Groningen, The Netherlands. Tel.: +31 503634327.
E-mail address: f.j.van.eerden@rug.nl (F.J. van Eerden).

we resort to multiscale molecular dynamics (MD) simulations. MD offers excellent possibilities to study lipid systems, as it allows to measure time and length scales which are difficult to access with experimental techniques. Membrane simulations have become common practice [17,18] and simulations of glycolipids are gaining popularity [19]. Previous MD studies in the thylakoid field include the simulation of a mixed MGDG/phosphocholine membrane [20] and a short (1 ns) simulation of PSII solvated in a bilayer composed of 73 thylakoid lipids, but lacking SQDG [21]. Recently a 10 ns all-atom simulation of photosystem II embedded in the thylakoid membrane was performed [22].

Here we simulate the thylakoid membrane of both higher plants and cyanobacteria. Our model of the thylakoid membrane is based on the experimental characterization of the thylakoid membrane by Sakurai et al. [3]. The cyanobacterial membrane composition is from *Thermosynechococcus vulcanus*, a thermophilic cyanobacterium, which is isolated from Japanese hotsprings and grows optimally around 330 K [23]. Surviving in such an environment requires a membrane that is still in a liquid-crystalline phase and not too leaky for protons at these elevated temperatures [24,25]. Increasing the amount of fully saturated fatty acids is one way in which prokaryotes do this [26]. The plant membrane composition is taken from *Spinacia oleracea* (spinach). In contrast to the cyanobacterial membrane, the plant membrane is strongly enriched in polyunsaturated lipids [3] that keep the thylakoid membrane fluid at physiological temperatures.

We combine coarse-grain (CG) and all-atom (AA) MD simulations to characterize the thylakoid membranes. Using the CG Martini model [27,28] we study the long time scale properties of the membranes and we analyze structural properties such as lateral lipid mixing and lipid tail order, as well as dynamic properties including diffusion of lipids and plastoquinone and plastoquinol co-factors. The cyanobacterial and plant membranes are compared to each other, and to membranes composed of more common phospholipids. Backmapping of representative CG configurations to all-atom models finally provides a fully atomistic view on the lipid organization of the thylakoid membrane.

2. Methods

2.1. System composition

The cyanobacterial membrane was modeled to the membrane composition of *T. vulcanus* and the plant membrane to the thylakoid composition of *S. oleracea* (spinach). The actual compositions were based upon the experimental characterization of the thylakoid membrane by Sakurai et al. [3]. Both cyanobacterial and plant membranes contain four major classes of lipids: phosphatidylglycerol (PG), digalactosyldiacylglycerol (DGDG), monogalactosyldiacylglycerol (MGDG) and sulfoquinovosyldiacylglycerol (SQDG). The difference between cyanobacterial and plant membranes is found mainly in the percentage of poly-unsaturated tails, which is increased in case of the plant membrane. The structure of the lipid head groups and tails that we included in our model are shown in Fig. 1. The compositions determined by Sakurai et al. [3] and the composition of our *in silico* membrane model are compared in Table 1. For the simulated membranes, we used a slightly higher proportion of PG headgroups than was found experimentally. This choice was made to increase the statistics in future studies on interaction of PG with PSII, which is believed to be functionally relevant [3]. The percentage of saturated SQDG is somewhat increased in our *in silico* membrane (80% in comparison to 70% in the experimental extract) due to a misrepresented particle bead type in one of our input files. Since the overall percentage of SQDG is only 25%, the difference is unlikely to significantly affect any of the results presented. The composition of the lipid tails of the *in silico* membranes is adapted to the resolution of the Martini model and differs therefore somewhat from the experimentally determined composition, see Table 1. The lipid tail composition also differs between the two membranes. The cyanobacterial membrane has mainly palmitoyl and oleoyl tails, whereas the plant membrane does not contain oleoyl, but has α-linolenoyl tails instead. The decision of which tails belong to which headgroup was based upon the resolution achievable with the Martini model and the work of Sakurai et al. [3]. Of note, the positional distribution of the fatty acids at the *sn*-1 and *sn*-2 positions in the
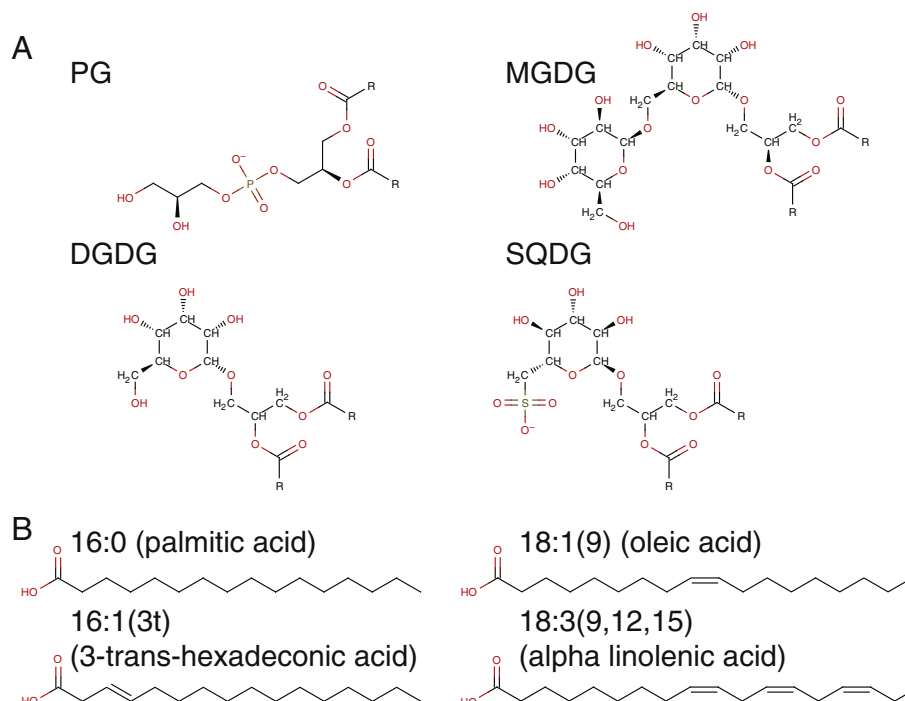
Fig. 1. Chemical structures of thylakoid lipid headgroups (A) and fatty acids (B).

Table 1
Lipid composition of cyanobacterial and plant membranes. Experimental composition, in mol%, according to Sakurai et al. [3]. Deviation of the experimental data is within 3%. nd, not detected. Simplified composition used in the in-silico models is given in parentheses.

Tail ↓ Head →	Cyanobacterial membrane				Plant membrane			
	PG	DGDG	MGDG	SQDG	PG	DGDG	MGDG	SQDG
16:0	47.9	43.6	45.1	62.0	15.6	6.7	3.1	49.2
18:0	8.9	2.5	3.9	8.0	0.4	0.6	0.6	2.3
saturated	(50)	(50)	(50)	(80)	(16)	(8)	(6)	(50)
16:1(7)	nd	nd	nd	nd	nd	0.2	0.3	1.4
16:1(9)	10.7	15.1	15.5	3.9	nd	nd	nd	nd
18:1(9)	26.3	28.1	27.9	20.9	nd	1.7	1.1	2.9
18:1(11)	6.2	10.7	7.6	5.2	nd	nd	nd	nd
unsaturated	(50)	(50)	(50)	(20)				
16:1(3t)	nd	nd	nd	nd	46.8	nd	nd	nd
trans-unsaturated					(50)			
16:3(7,10,13)	nd	nd	nd	nd	nd	4.1	13.6	1.0
18:2(9,12)	nd	nd	nd	nd	2.2	2.4	3.1	6.3
18:3(9,12,15)	nd	nd	nd	nd	35.0	84.3	78.2	36.9
poly-unsaturated					(34)	(92)	(94)	(50)
total	**6.1**	**25.6**	**43.5**	**24.8**	**12.6**	**25.1**	**40.1**	**15.2**
	(10)	**(25)**	**(40)**	**(25)**	**(15)**	**(30)**	**(40)**	**(15)**

cyanobacterial membrane is different than in most lipids [29,30]. The oleoeic tail is connected to the sn-1 position and the palmitic tail to the sn-2 position, except for SQDG headgroups. For the plants it was assumed that the trans-unsaturated tails and the poly-unsaturated tails are connected to the sn-1 position. In real plant membranes the tail connectivity might be more complicated, see e.g. [31,32].

The final composition of each of the membrane models is as follows. The cyanobacterial membrane consists out of a mixture of five different lipids, namely 204 18:1(9)-16:0 PG, 512 18:1(9)-16:0 DGDG, 818 18:1(9)-16:0 MGDG, 204 18:1(9)-16:0 SQDG and 306 di16:0 SQDG lipids, 2044 lipids in total. These lipids were solvated in 21 498 CG water beads representing 85 992 water molecules, 850 sodium ions and 136 chloride ions. The plant system is composed of seven different lipids, namely 102 16:1(3t)-16:0 PG, 204 16:1(3t)-18:3(9,12,15) PG, 102 18:3(9,12,15)-16:0 DGDG, 512 di18:3(9,12,15) DGDG, 102 18:3(9,12,15)-16:0 MGDG, 716 di18:3(9,12,15) MGDG and 306 18:3(9,12,15)-16:0 SQDG lipids, totaling 2044 lipids. The plant membrane was solvated with 21 600 CG waters representing 86 400 water molecules, 748 sodium ions and 136 chloride ions. The added ions neutralize the charges of the PG and SQDG headgroups and the NaCl provides an overall salt concentration of approximately 88 mM (excluding counter ions). The unit cell of both the cyanobacterial and plant membrane measured 25.5 × 25.5 nm in the lateral (x,y) dimensions and 15 nm in the z dimension at the start of the simulation.

Smaller systems, which exhibit less undulations, were used in addition for the measurement of structural properties such as area compressibility moduli, area per lipid, and order parameters. The smaller cyanobacterial system is composed of 284 lipids, 28 18:1(9)-16:0 PG, 72 18:1(9)-16:0 DGDG, 114 18:1(9)-16:0 MGDG, 28 18:1(9)-16:0 SQDG and 42 di16:0 SQDG lipids, solvated in 4053 CG water beads (16 212 water molecules), 123 sodium and 25 chloride ions. The plant system is composed of 284 lipids, 14 16:1(3t)-16:0 PG, 28 16:1(3t)-18:3(9,12,15) PG, 14 18:3(9,12,15)-16:0 DGDG, 72 di18:3(9,12,15) DGDG, 14 18:3(9,12,15)-16:0 MGDG, 100 di18:3(9,12,15) MGDG and 42 18:3(9,12,15)-16:0 SQDG lipids, solvated with 4088 CG water beads (16,352) water molecules, 110 sodium and 26 chloride ions. A pure POPC membrane served as a control, and is composed of 288 lipids, 4469 CG water beads (17 876 water molecules), 27 sodium and 27 chloride ions. The unit cell of the smaller membrane patches measured 9.5 × 9.5 × 9.0 nm in (x, y, z) dimensions at the start of the simulation.

To study the propensity of the membranes to undergo a phase transition toward the inverted hexagonal phase a third system was used composed of two stacked bilayers with solvent in between. For the cyanobacterial system each of these bilayers contains 644 lipids,

namely 64 18:1(9)-16:0 PG, 162 18:1(9)-16:0 DGDG, 258 18:1(9)-16:0 MGDG, 64 18:1(9)-16:0 SQDG and 96 di16:0 SQDG lipids. For the plant system each bilayer contains 644 lipids, 32 16:1(3t)-16:0 PG, 64 16:1(3t)-18:3(9,12,15) PG, 32 18:3(9,12,15)-16:0 DGDG, 162 di18:3(9,12,15) DGDG, 32 18:3(9,12,15)-16:0 MGDG, 226 di18:3(9,12,15) MGDG and 96 18:3(9,12,15)-16:0 SQDG lipids. Counterions were added to these systems, which were solvated with a varying amount of water, the NaCl concentration was adjusted towards approximately 85 mM (excluding counter ions). The unit cell of both systems measured 14.0 × 14.0 × 13.0 nm in (x, y, z) dimensions at the start of the simulation.

To study the behavior of plastoquinol (PL9ol) and plastoquinone (PL9on) in the thylakoid membrane, two additional systems were setup. These systems contained either four PL9ols or four PL9ones embedded in a cyanobacterial bilayer composed of 72 18:1(9)-16:0 PG, 180 18:1(9)-16:0 DGDG, 288 18:1(9)-16:0 MGDG, 108 18:1(9)-16:0 SQDG and 72 di16:0 SQDG lipids. The bilayer was solvated in 21 258 CG water beads (equivalent to 85 032 water molecules) and neutralized by 252 sodium ions.

2.2. CG simulation details

The Martini lipid force field [28] was used to model the interactions. The Martini model has been successful in describing membrane structural properties (e.g. [33,34]), including membranes with complex lipid composition [35]. CG topologies of representative lipids are shown in Fig. 2. The specific parameters of the glycolipid headgroups were taken from López et al. [36], but were slightly modified to better match the atomistic results and increase the stability of the lipids. In particular, the GA1, GB1 and GB2 beads of the DGDG headgroup were
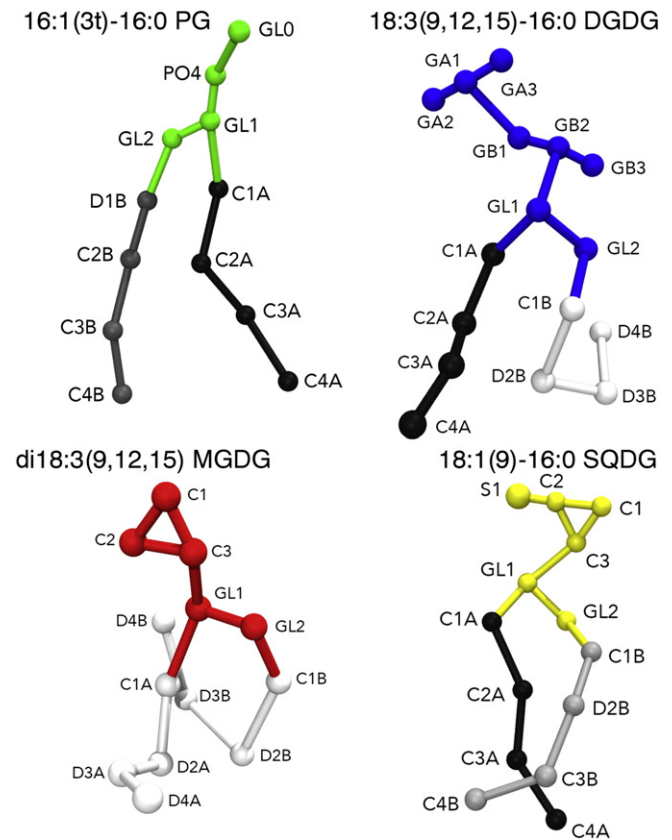
Fig. 2. CG topologies of representative lipids of the thylakoid membrane. PG head group beads are shown in green, DGDG in blue, MGDG in red, and SQDG in yellow. Fully saturated tails are depicted black, triple unsaturated tails in white, single unsaturated tails in light gray and trans unsaturated tails in dark gray. The labels are used for reference later in the main text.

changed from respectively P2, N0 and P4 to SP2, SN0 and SP2 type beads. To increase the stability of the DGDG and SQDG headgroups the constraints between GA1-GA2, GA1-GA3, GB1-GB2 and GB2-GB3 of the DGDG headgroup and between the S1-C2 beads of the SQDG headgroup were changed into bonds with a force constant of 30,000 kJ mol^{-1}. The parameters for plastoquinone and plastoquinol were taken from De Jong e t al. [37]. All lipid tails were modeled by four CG beads, representative of 15–18 carbons in the Martini model. The palmitoyl chain was modeled by four C1 beads, the oleoyl chain by three C1 beads and one C3 bead, with the C3 bead being the third counting from the methyl terminal bead. The α-linolenoyl chain was modeled with three C4 beads and a C1 bead at the carboxyl terminus. Bonded beads were kept at an equilibrium distance of 0.47 nm with a force constant of 1250 kJ mol^{-1} using a harmonic potential. The angles between three consecutive tail beads were likewise constrained by a harmonic potential with an equilibrium angle of 180° and a force constant of 25 kJ mol^{-1}. In order to mimic the more flexible nature of α-linolenoyl the angles between the three C4 beads were set to 100° with a force constant of 10 kJ mol^{-1}. The trans-3-hexadecenoic acid was modeled as a C3 bead at the carboxyl terminus, which represents the double bond, and three C1 beads. The angle of the C3 bead was set to 180° with an increased force constant of 45 kJ mol^{-1} to account for the trans orientation.

All simulations were performed with the GROMACS 4.5.5 MD package [38], with standard parameter settings associated with the Martini force field [28]. Membranes were pre-assembled using the Insane script [39]. After energy minimization of the systems using a steepest decent algorithm, the systems were simulated using a leap-frog integrator with a time step of 10 fs. Systems were simulated in the isothermal-isobaric (NpT) ensemble. The temperature was kept constant using the Berendsen thermostat with a coupling constant τ_t = 2.0 ps [40]. Lipids and solvent were coupled separately to avoid heat flow. The pressure was semiisotropically coupled to an external bath of p = 1 bar with a coupling constant of τ_p = 1.0 ps and compressibility of χ = 3.0×10^{-4} bar^{-1} using the Berendsen barostat [40]. Electrostatic interactions were calculated using a shifted potential with a cut off of 1.2 nm and a dielectric constant of 15. Van der Waals interactions were also calculated using a shifted potential with a cut off of 1.2 nm and a switch at 0.9 nm. The large membrane patches were simulated for 10 μs and the smaller patches for 3.8 μs, the membrane with PL9on was simulated for 3 μs and the membrane with PL9ol for 3.5 μs, not taking into account a speed-up due to the CG nature of the interactions. This speed-up factor is estimated to be about a factor of four based on lateral diffusion of lipids and membrane proteins [41]. The first 1 μs was considered equilibration time in all cases. For investigating the phase behavior of the membranes the run parameters were identical, except that a τ_p of 1.2 ps and a τ_t of 0.5 ps were used and the compressibility was set to $\chi = 1.0 \times 10^{-5}$ bar^{-1}, following Ref. [42].

2.3. Atomistic simulation details

In order to assess the accuracy of the CG membranes, small patches of equilibrated CG cyano and plant membranes were transformed to fully atomistic membranes. The cyanobacterial system contained 160 lipids and was composed of 16 18:1(9)-16:0 PG, 40 18:1(9)-16:0 DGDG, 64 18:1(9)-16:0 MGDG, 16 18:1(9)-16:0 SQDG and 24 di16:0 SQDG lipids, solvated in 2238 CG water beads, which were transformed into 8952 SPC waters, 69 sodium and 13 chloride ions. The plant membrane also contained 160 lipids, 8 16:1(3t)-16:0 PG, 16 16:1(3t)-18:3(9,12,15) PG, 8 18:3(9,12,15)-16:0 DGDG, 40 di18:3(9,12,15) DGDG, 8 18:3(9,12,15)-16:0 MGDG, 56 di18:3(9,12,15) MGDG and 24 18:3(9,12,15)-16:0 SQDG lipids. The system further contained 2924 CG water beads, which were transformed into 11 696 atomistic waters, 65 sodium and 17 chloride ions. The backmapping was performed as described by Rzepiela e t al. [43], involving a 60 ps restrained simulated annealing. The annealing time step was set to 2 fs, the restraining

force constant to 12 000 kJ mol^{-1}, and the initial capping force to 15 000 kJ mol^{-1} nm^{-1} that increased by 100 kJ mol^{-1} nm^{-1} ps^{-1}. The initial temperature of the lipids was set to 1300 K and of the solvent to 400 K, both of them were decreased to 300 K during the simulated annealing. The annealing method was single and the radius of the CG water was set to 0.21 nm. After the simulated annealing the atomistic system was simulated using the GROMOS 53a6 force field [44]. The parameters for the atomistic lipids were based upon the GROMOS force field and were kindly provided by Dr. A.H. De Vries (personal communication, 2012). Dihedral restraints were used to keep the sugar rings of the glycolipids in the right stereoisomer. To prevent excessive spinning of hydrogens in the sugar alcohol groups, 3 u was transferred from the oxygen to the hydrogen in this group, giving rise to an oxygen mass of 12.9994 u and a hydrogen mass of 4.008 u. The time step was set to 1.5 fs. The temperature was kept constant using the Berendsen thermostat with a coupling constant τ_t = 2.0 ps [40]. Lipids and solvent were coupled separately to avoid heat flow. The pressure was semiisotropically coupled to an external bath of 1 bar with a coupling constant of τ_p = 0.1 ps and compressibility of $\chi = 4.6 \times 10^{-5}$ bar^{-1} using the Berendsen barostat [40]. The electrostatics were calculated using particle-mesh Ewald with a cut-off of 1.4 nm, using a Fourierspacing of 0.12 [45, 46]. A single cut-off of 1.4 was used for Van der Waals interactions. In total 1.2 μs of the cyanobacterial membrane was simulated and 1.0 μs of the plant membrane. Analysis of the atomistic system was done after reverse mapping it to a CG system. For the calculation of the area per lipid and the compressibility the first 400 ns were discarded as equilibration.

2.4. Analysis details

To characterize the mixing behavior of the lipids, the normalized amount of contacts between different lipid species was calculated. Lipids were considered to be in contact with each other when their GL1 beads (representing the glycerol moiety) resided within a radius of 0.8 nm, which corresponds with the first solvation shell in the Martini model. The same procedure was used to calculate contacts between lipid head groups and solvent: A head group bead was considered to be in contact with a solvent bead when they where within a distance of 0.8 nm. The lateral diffusion of lipids and cofactors was calculated from the mean square displacement (MSD) of the molecules in the membrane plane, $MSD = \langle |r(t + t_0) - r(t_0)|^2 \rangle$ where r represents the position of the molecular center-of-mass, and angular brackets denote an average over both time t and the number of molecules examined. The section of the MSD curve where $MSD \sim t$ represents normal diffusion and this part was fitted to $y = 4Dt + c$, to obtain D, the lateral diffusion constant. To quantify membrane order, the segmental lipid order parameter was calculated according to $S = \left\langle \frac{3\cos^2\theta - 1}{2} \right\rangle$ where Θ is the angle between the bond vector of two consecutive tail beads and the z-axis. The area compressibility is calculated as described by Feller and Pastor [47]: $K_A = \frac{kTA_0}{N\langle (A - A_0)^2 \rangle}$, where K_A is the compressibility modulus, T is the temperature, A the surface area per lipid, A_0 the average surface area per lipid and N the amount of lipids per monomer. The thickness of the membranes was determined by measuring the distance between the GL1 beads of the two leaflets, using the Gromacs tool g_dist [38]. The conformations sampled by cofactors simulated in a bilayer system were analyzed using a cluster analysis algorithm described by Daura et al. [48] and implemented in the Gromacs tool g_cluster. An RMSD cut-off of 0.15 nm was used in the analysis.

3. Results and discussion

3.1. Lateral mixing of thylakoid lipids

In this section we consider the lateral organization of the thylakoid membrane models, based on simulations of membrane patches
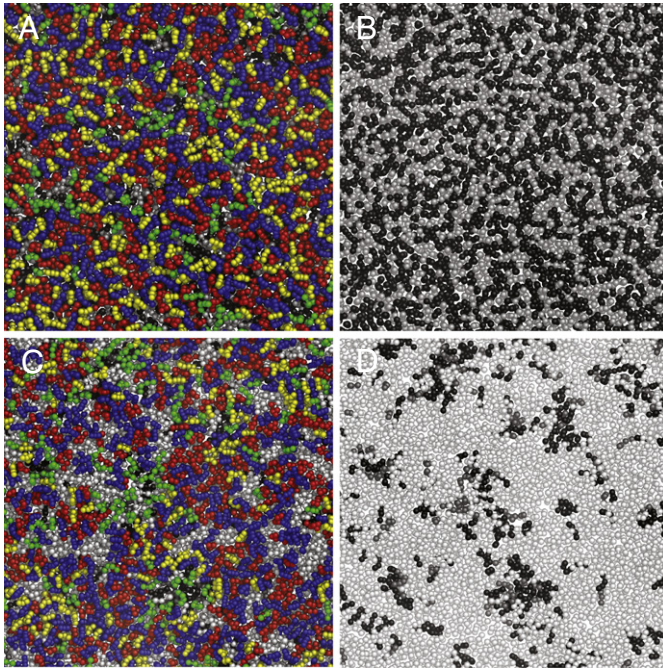
Fig. 3. Lateral organization of thylakoid membranes. Top views of the cyanobacterial membrane (A,B) and the plant membrane (C,D) are shown, both at T = 293 K. In (B,D) only the tail beads are visualized. PG headgroups are in green, DGDG headgroups in blue, MGDG headgroups in red, SQDG headgroups in yellow. Tails are colored according to the degree of saturation 16:0 tails are black, 16:1(3t) are dark gray, 18:1(9) are colored light gray and 18:3(9,12,15) are colored white.

composed of 2044 lipids. Fig. 3 shows representative configurations of both the cyanobacterial and plant thylakoid membranes at T = 293 K, obtained after 38 and 56 μs CG MD simulation, respectively. From these snapshots is it clear that the global mixing of the lipids is rather homogeneous. No large-scale phase separation is observed, although heterogeneities on the nanoscale do seem to occur.

The lipid mixing was further quantified by determining the lipid–lipid contact percentages as explained in the Methods section. The results are summarized in Table 2 (cyanobacterial) and Table 3 (plant). The contact percentages in the cyanobacterial membrane confirm the visual impression that the lipid head groups in general mix well. However, the data in Table 2 reveal that the contacts of PG with SQDG are significantly reduced, with only 6% contacts formed whereas 10% would be expected from random mixing, an effective reduction of 40%. PG and SQDG both carry a negatively charged headgroup and might be expected to repel each other. Indeed, SQDG–SQDG pairs are

also somewhat reduced. PG–PG pairs, however, are observed to occur at normal (i.e. random) level. We attribute this to the smaller PG headgroup which is able to bridge a counterion in between to neutralize the charge. This bridging is not possible for the much larger headgroup of SQDG. Another significant deviation from random mixing is the self-interaction of DGDG with only 17% contacts observed compared to 25% expected based on its molar fraction. The reason is likely steric hindrance caused by the big disaccharide head group. There were no major differences between the contact percentages of the CG membrane at 293 K and at 328 K. In the short all-atom simulation performed at 328 K after a backmapping procedure, the level of mixing remained similar to that of the CG membrane (cf. Table 2). Noticeable exceptions are contacts between PG–PG, SQDG–SQDG and MGDG–PG. In the atomistic membrane the anionic PG lipids seem to repel each other much more. The same is true, to a lesser extent, for the anionic SQDG lipids. The PG–MGDG interactions are increased at the atomistic level, possibly to compensate for the decreased PG–PG interactions. The backmapped membrane at 293 K adopted a gel phase, preventing further lipid rearrangements, and was not further analyzed. Note, this phase transition does not take place in the CG membrane, as the Martini model is known to underestimate the phase transition temperature of saturated lipids [36].

In the plant membrane the behavior of the lipids is more complex due to the greater variety in fatty acids. The snapshot (Fig. 3C) shows global mixing, but clear evidence for nanoscale inhomogeneities can be detected, especially when color coded according to lipid tail type (Fig. 3D). This can also be inferred from the lipid–lipid contact percentages for the plant membrane, shown in Table 3. Looking at the contact percentages of lipids with fully saturated tails (counting the trans-unsaturated tail as such), an increased number of contacts can be appreciated. In contrast, mixing of lipids with fully saturated versus polyunsaturated tails is significantly reduced, for instance 16:1(3t)-16:0 PG has only 14% of its contacts with di18:3(9,12,15) MGDG, despite the latter being the most abundant lipid in the plant membrane at 35% mol fraction. Some tendency toward clustering of lipids with polyunsaturated tails can also be appreciated, as reflected by an increase in contacts between di18:3(9,12,15) MGDG and di18:3(9,12,15) DGDG (47% versus 35% for random mixing). This clustering effect is not seen for DGDG–DGDG pairs however, due to the opposing effect coming from the bulky DGDG headgroup, as also observed in the cyanobacterial membrane. In case of PG lipids in the plant membrane, the tendency of the saturated tails to cluster and the possibility for the small head group to form ion mediated neutral complexes combine, leading to noticeable PG nanodomains (cf. Fig. 3C). Self-contacts between 16:1(3t)-16:0 PG are enhanced to 23% compared to 5% expected from a random organization. In the atomistic plant membrane the PG–PG, as well as the SQDG–SQDG, interactions are reduced, in line with the results for the cyanobacterial

Table 2
Contact percentages between various lipids in the cyanobacterial membrane. The standard error for the CG simulations is below 0.1%. For the calculation of the standard error it was assumed that every 250 ns of each leaflet counts as an independent observation. Percentages between parentheses in the rows after the lipid names indicate the total share of that lipid in the system. Contact percentages are normalized with respect to the total number of contacts formed by the lipids in the 1st row. Relative deviations in contact percentages of more than 20% from what can be expected from random mixing are shown in bold face (CG only). Contact percentages that showed a large shift during the short atomistic simulations are marked with *. CG contacts percentages are from the simulation at 293 K, the differences between those with the contact percentages of the simulation at 328 K are within 2%. The CG contact percentages are from the simulation at 328 K.

		18:1(9)-16:0 PG	18:1(9)-16:0 DGDG	18:1(9)-16:0 MGDG	18:1(9)-16:0 SQDG	di16:0 SQDG
18:1(9)-16:0 PG(10%)	CG	10%*	10%	8%*	**6%**	**6%**
	AA	3% ± 2	10% ± 1	16% ± 1	8% ± 2	7% ± 1
18:1(9)-16:0 DGDG (25%)	CG	27%	**17%**	25%	27%	26%
	AA	20% ± 2	20% ± 2	23% ± 1	26% ± 3	30% ± 3
18:1(9)-16:0 MGDG (40%)	CG	44%*	45%	39%	46%	46%
	AA	61% ± 3	42% ± 2	35% ± 1	50% ± 3	45% ± 2
18:1(9)-16:0 SQDG (10%)	CG	8%	12%	11%	8%*	8%
	AA	7% ± 1	10% ± 1	11% ± 1	4% ± 2	8% ± 1
di16:0 SQDG	CG	**11%**	17%	17%	13%	14%*
(15%)	AA	9% ± 2	18 % ± 1	15% ± 1	12% ± 2	10% ± 3

Table 3

Contact percentages between various lipids in the plant membrane. The standard error of the CG systems is below 0.2%. For the calculation of the standard error it was assumed that every 250 ns of each leaflet counts as an independent observation. Percentages between parentheses in the rows behind the lipid names indicate the total share of that lipid in the system. Contact percentages are normalized with respect to the total number of contacts formed by the lipids in the 1st row. Relative deviations in contact percentages of more than 50% from what can be expected from random mixing are shown in bold face (CG only). Contact percentages that showed a large shift during the short atomistic simulations are marked with *.

		16:1(3t)-16:0 PG	16:1(3t)-18:3(9,12,15) PG	18:3(9,12,15)-16:0 DGDG	di18:3(9,12,15) DGDG	18:3(9,12,15)-16:0 MGDG	di18:3(9,12,15) MGDG	18:3(9,12,15)-16:0 SQDG
16:1(3t)-16:0 PG	CG	**23%***	7%	**11%**	**2%**	**9%***	**2%***	5%*
(5%)	AA	11% ± 4	4% ± 2	7% ± 4	4% ± 1	1% ± 1	7% ± 1	10% ± 1
16:1(3t)-18:3(9,12,15)	CG	13%	11%*	12%	8%	10%*	7%	7%
PG (10%)	AA	7% ± 3	20% ± 3	12% ± 3	8% ± 2	20% ± 4	11% ± 1	6% ± 1
18:3(9,12,15)-16:0	CG	**12%***	**8%**	5% *	**3%**	**7%**	4%	**8%**
DGDG (5%)	AA	6% ± 3	6% ± 1	10% ± 4	2% ± 1	3% ± 2	6% ± 1	5% ± 1
di18:3(9,12,15) DGDG	CG	**10%**	23%	**11%**	20%	17%	28%	21% *
(25%)	AA	16% ± 3	18% ± 4	10% ± 4	17% ± 2	17% ± 4	28% ± 2	31% ± 3
18:3(9,12,15)-16:0	CG	**11% ***	7%	**9%***	4%	**8% ***	4%	**8%**
MGDG (5%)	AA	1% ± 1	9% ± 2	3% ± 2	4% ± 1	1% ± 1	4% ± 1	10% ± 3
di18:3(9,12,15) MGDG	CG	**14%***	31%	27%	47%	26%	41%	33%
(35%)	AA	39% ± 3	36% ± 3	42% ± 6	45% ± 2	28% ± 3	32% ± 2	33% ± 2
18:3(9,12,15)-16:0	CG	18%	14%	26%*	16%	**24%**	15%	18% *
SQDG (15%)	AA	21% ± 3	8% ± 1	15% ± 5	19% ± 1	29% ± 8	13% ± 1	5% ± 1

membrane. The all-atom simulations furthermore point to increased interactions between lipids with one or two saturated tails and lipids with two polyunsaturated tails. For instance, 16:1(3t)-16:0 PG contacts with di18:3(9,12,15) MGDG are increased from 14% to 39%. At the same time, lipids containing a saturated tail show a smaller tendency of clustering with each other, exemplified by a drop of contacts for 18:3(9,12,15)-16:0 DGDG with 18:3(9,12,15)-16:0 SQDG from 26% to 15%. In both cases, the atomistic results are closer to that expected from a random mixture, a trend that appears more general. A number of other changes can be appreciated from Table 3, however, mostly concerning the interactions between components present at low mol fraction (5%).

Taken together, our data show that the thylakoid membrane comprises a largely homogeneous mixture of the constituent glycolipids. Domain formation is not observed. Some tendencies to non-ideal mixing exist, most notably the clustering of PG lipids especially in the plant membrane, and the co-aggregation of lipids with either fully saturated or fully polyunsaturated tails.

3.2. The plant membrane is more fluid than the cyanobacterial membrane

To characterize the thylakoid membranes further, we compared a number of structural measures, namely the area per lipid, bilayer thickness, and area compressibility (see Methods). The results are summarized in Table 4. Our data show that the cyanobacterial membrane is more densely packed, thicker and has a higher compressibility modulus than the plant membrane. The higher apparent fluidity of the plant membrane is attributed to the presence of the polyunsaturated lipid tails. In nature, *T. vulcanus* is found in an environment with harsh conditions and grows optimally at 330 K [23], explaining the need for a more robust membrane. Increasing the temperature in our simulations from 293 K to 328 K, we observe a slight thinning of the cyanobacterial

Table 4

Structural properties of thylakoid membranes. Area per lipid (A), compressibility modulus (KA), and membrane thickness (d) of the various membranes at both CG and AA resolution. The standard error is given between parentheses, and was estimated using block averaging as implemented in the Gromacs tool g_analyze. [a]The cyanobacterial membrane at AA resolution adopted a gel phase and could not be equilibrated.

		A (nm²)	K_A (mN/m)	d (nm)
Cyanobacterial, 293 K	CG	0.58 (0.0002)	589 (28)	3.3 (0.0007)
	AA[a]	–	–	–
Cyanobacterial, 328 K	CG	0.62 (0.0002)	426 (10)	3.2 (0.0007)
	AA	0.64 (0.001)	350 (27)	3.0 (0.007)
Plant, 293 K	CG	0.66 (0.0006)	240 (16)	2.9 (0.0007)
	AA	0.66 (0.003)	311 (125)	2.8 (0.015)
POPC, 293 K	CG	0.64 (0.0002)	412 (12)	3.2 (0.002)
POPC, 328 K	CG	0.69 (0.0002)	396 (13)	3.1 (0.0007)

membrane and increase in area per lipid, but nowhere near the values obtained for the plant membrane. Our results for the CG model are consistent with the values obtained after backmapping to all-atom resolution. The cyanobacterial membrane is slightly thinner at the atomistic resolution. The atomistic bacterial membrane appeared to be in gel phase at 293 K, as was mentioned above. A reference POPC bilayer shows structural parameters somewhere in between those of the plant and cyanobacterial membrane.

To quantify the order of the thylakoid membranes, we calculated the segmental lipid tail order parameters (see Methods). The order parameter profiles are shown in Fig. 4, for the cyanobacterial membrane at both 293 K and 328 K, and for the plant membrane at 293 K. Order parameters for the CG POPC membrane are also included for reference. In line with expectations, the order parameters from the thylakoid membranes form two basic clusters: higher order parameters for the saturated tails and lower order parameters of the (poly) unsaturated tails. The difference between these tails gets smaller for the cyanobacterial membrane at increased temperature. Overall, the lipids in the plant membrane are less ordered than the lipids in the cyanobacterial membranes. This is especially true for the α-linolenoyl tails, but also the palmitoyl tails are less ordered in the plant membrane. The reference POPC membrane shows an intermediate order. These results are consistent with the differences in structural parameters as discussed above. In the plant membrane, the tail order of the PG lipids is different from the DG lipids. Noticeable is the relative high order of the tails of 16:1(3t)-16:0 PG, with the two tails showing almost the exact same degree of order. The α-linolenoyl tail of 16:1(3t)-18:3(9,12,15) PG, however, is similarly ordered compared to the other α-linolenoyl tails and the trans-hexadeconic tail has a similar ordering as the palmitoyl tails of the glycolipids. The reason for this behavior might be related to the clustering tendency of PG lipids in the plant membrane. As shown in the preceding section, 16:1(3t)-16:0 PG has a high tendency to cluster, which could result in ordering of the lipid chains. Consistent with this idea, the tails of 16:1(3t)-18:3(9,12,15) PG show similar order as the other glycolipid tails and better mixing with the other lipids as well (cf. Table 3).

The atomistic order parameter profiles show the first bond index to be much less ordered compared to the CG profiles. In atomistic simulations of pure glycolipids membranes a similar ordering has been observed and is possibly a result of a lower accessibility to the glycerol groups for water (Dr. A.H. De Vries, unpublished results). The Martini model does not have the resolution to capture these differences. For the interior part of the membrane (bonds 2–4), the atomistic order profiles are very similar to the CG ones, exceptions are the third bond of the 18:3 tails, which is a bit more ordered in the atomistic simulations,
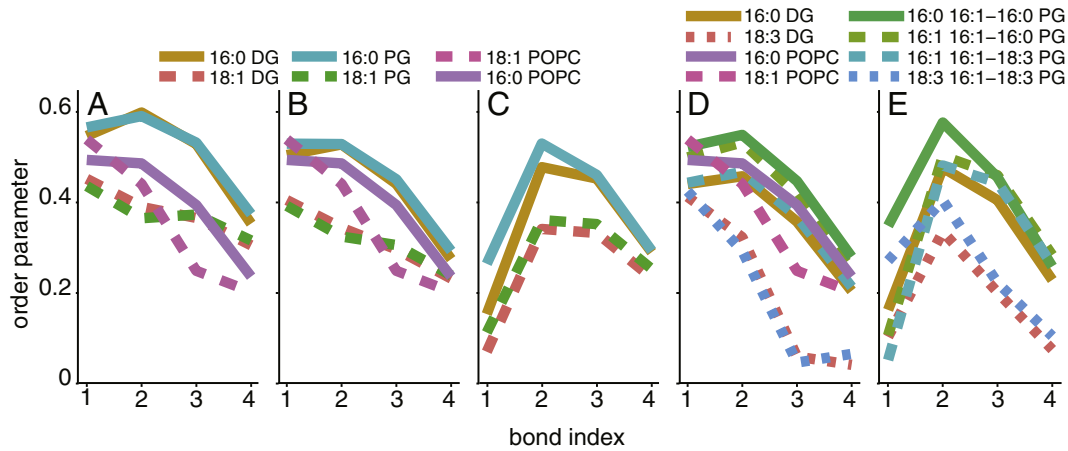
Fig. 4. Thylakoid membrane order parameter profiles. Profiles are shown for the cyanobacterial membrane at CG resolution at 293 K (A), 328 K (B), and AA at 328 K (C) and the plant membrane, CG at 293 K (D) and AA at 328 K (E). For reference purposes the order profiles of a POPC membrane at 293 K have been added to the CG data. Increasing bond indices represent respectively the bond between the GL bead and the first tail bead, the first and second tail bead, the second and third and the third and fourth tail bead. Order parameter profiles are distinguished between PG lipids and glycolipids (denoted DG); within these classes results are averaged over all chemically identical lipid tails. Solid lines stand for fully saturated lipids, dashed lines for mono-unsaturated lipids (both cis and trans unsaturation) and dotted lines for polyunsaturated lipids.

and the tails of 16:1(3t)-16:0 PG in the plant membrane. In the CG membrane the two fatty acids of 16:1(3t)-16:0 PG have an identical ordering, but in the atomistic membrane the palmitoyl tail is more ordered than the trans unsaturated tail, in correspondence with the fact that 16:1(3t)-16:0 PG has a much lower tendency to cluster atomistically.

Next to the structural characterization of thylakoid membrane fluidity, we measured the diffusivity of the constituent lipids. The long-term diffusion constant was obtained from the mean squared displacement of the lipids as explained in the Methods section. The results are summarized in Table 5.

Two main observations can be made. First, the spread in diffusion constants between the different lipids in the same membrane is very limited. Within the error bars, all lipids diffuse at the same speed. Given the collective nature of the diffusion process and the overall homogeneity of the thylakoid membranes, a larger spread in diffusivities is not expected. The only exceptions are the somewhat faster diffusion rate of the polyunsaturated lipids versus the saturated lipids in the plant membrane and the low diffusion constant of 16:1(3t)-16:0 PG.

Table 5
Lipid lateral diffusion constants in the plant and cyanobacterial membranes. Standard errors are given in parenthesis. The error was estimated considering blocks of 250 ns, as well as the two leaflets, as independent samples. Note that the absolute value of diffusion rates obtained with CG models has to be interpreted with care due to a general speedup of the dynamics. For lipid diffusion, a speedup factor of about four has been reported [41], implying that realistic diffusion rates are four times lower than those reported here. The AA cyanobacterial membrane is in the gel phase and reliable diffusion constants could not be obtained.

	D_{CG} (µm²/s) 293 K	D_{AA} (µm²/s) 293 K	D_{CG} (µm²/s) 328 K	D_{AA} (µm²/s) 328 K
Cyanobacterial membrane				
18:1(9)-16:0 PG	23 (1.1)		55 (2.7)	1.4 (0.2)
18:1(9)-16:0 DGDG	18 (0.6)		47 (1.6)	1.4 (0.2)
18:1(9)-16:0 MGDG	21 (0.6)		52 (1.4)	1.7 (0.1)
18:1(9)-16:0 SQDG	20 (0.9)		53 (2.9)	1.7 (0.2)
di16:0 SQDG	20 (0.7)		51 (1.6)	1.5 (0.1)
Plant membrane				
16:1(3t)-16:0 PG	19 (2.1)	0.3 (0.07)		
16:1(3t)-18:3(9,12,15) PG	34 (1.9)	0.3 (0.06)		
18:3(9,12,15)-16:0 DGDG	28 (1.8)	0.4 (0.07)		
di18:3(9,12,15) DGDG	32 (1.2)	0.3 (0.05)		
18:3(9,12,15)-16:0 MGDG	32 (1.8)	0.4 (0.09)		
di18:3(9,12,15) MGDG	34 (1.2)	0.4 (0.04)		
18:3(9,12,15)-16:0 SQDG	32 (1.1)	0.3 (0.03)		
Reference				
POPC	43 (1.0)		95 (1.9)	

Experimentally, it has been shown that a higher unsaturation grade results in higher diffusion constants [49], consistent with our findings. The low diffusion constant of 16:1(3t)-16:0 PG is likely to be a result of its more ordered tails caused by its tendency to cluster (cf. Tables 2 and 3 and Fig. 4). Second, the plant lipids diffuse significantly faster than the cyanobacterial lipids at 293 K, which is likely due to their higher unsaturation grade and associated increase in membrane area (cf. Table 4). However, compared to the POPC membrane the lipids in both thylakoid membranes are slowed down. We contribute this to the presence of the bulky sugar head groups, which hamper the diffusion process. In all-atom simulations, a similar decrease in lipid diffusion in glycolipid membranes has been reported [50]. In line with this, we find the lowest diffusion constants for the DGDG lipids, which have the largest head group. Note that CG lipids experience a smoother energy landscape than atomistic lipids, which results in higher diffusion constants. The speedup factor has been estimated to be about four [41]. This might largely account for the five times higher diffusion constant of the POPC lipids compared with the experimentally determined diffusion constant of POPC lipids, D = 8 µm²/s at T = 298 K [51]. The diffusion constants of the atomistic cyanobacterial lipids at 328 K are about half of those reported by Ogata et al. in their atomistic simulation of photosystem II, at 300 K [22]. However the thylakoid membrane modeled by Ogata et al. contains more polyunsaturated lipids, which influences the diffusivity of the system. Besides, the simulation time is restricted to 8 ns, which is too short to accurately determine diffusion rates.

Together, our analysis of structural and dynamic properties points to a much more fluid character of the plant membrane compared to the cyanobacterial membrane, even if the two membranes are compared at their respective physiological temperatures. Due to the large conformational freedom of the polyunsaturated tails present in the plant membrane, the area per lipid is increased and membrane thickness decreased. The plant membrane is also less ordered, more easily compressible, and shows increased diffusivity of the lipids.

3.3. Cross sections of the thylakoid membranes

Having established an overall decrease in fluidity and order of the cyanobacterial membrane versus the plant membrane, next we turn to the cross sectional characterization of the thylakoid membranes by means of electron density profiles (Fig. 5) and graphical snapshots of the membrane/water interface (Fig. 6). The electron density profiles reveal an overall membrane organization similar to that of a typical membrane such as the POPC membrane, with the polar headgroups pointing toward the aqueous phase and lipid tail segments shielded from water.
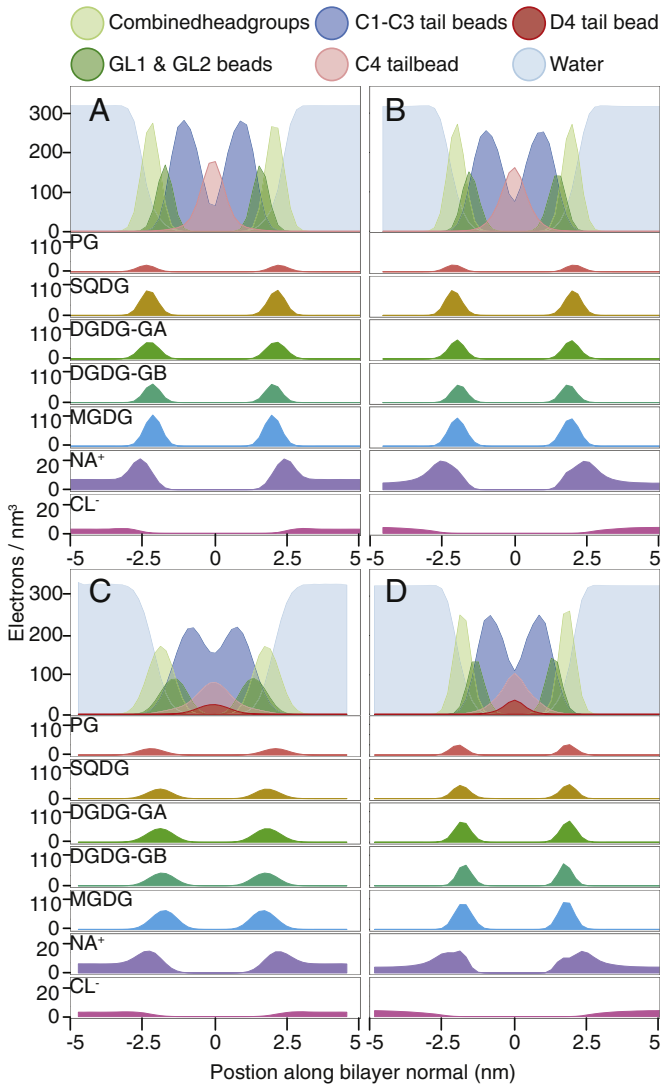
Fig. 5. Electron density profiles of thylakoid membranes. Panels show the profiles of the CG cyanobacterial membrane at 328 K (A), AA cyanobacterial membrane at 328 K (B), the CG plant membrane at 293 K (C), the AA plant membrane at 293 K (D). The upper graphs show the electron density of the combined headgroups, the glycerol backbone (GL1, GL2), the first three tail beads (C1–C3), the last tail bead of saturated (C4) or unsaturated (D4) tails and water. The lower panel section shows the electron densities for the different headgroups and the ions, with separate plots for the first (GA) and the second (GB) sugar ring of DGDG. To obtain AA profiles that could be easily compared to the CG profiles, the AA trajectory was mapped to CG resolution.

Fig. 6. Cross-sectional organization of thylakoid membranes. Snapshots obtained from the smaller systems used to calculate the electron densities and order parameters. (A) CG cyanobacterial membrane at 328 K, (B) AA cyanobacterial membrane at 328 K, (C) CG plant membrane at 293 K, (D) AA plant membrane at 293 K. The coloring of the lipids is identical as in Fig 3. Water is colored light blue, sodium ions colored pink, and chloride ions are lime colored.

The glycerol groups reside at the interface and are still partially solvated. Water penetration is somewhat larger in the plant membrane. In all membranes, the characteristic density dip in the middle of the membrane is observed. A number of additional features pertaining to the thylakoid membrane organization are worth pointing out. In general, the electron density peaks of the plant membrane are broader and are located more to the center of the bilayer compared to the cyanobacterial membrane, in line with the thinner and more disordered nature of the plant membrane discussed above. Despite the smaller thickness of the plant membrane, the spread of the tail beads is much larger. This is due to the ability of the poly-unsaturated lipids to backfold toward the interface and has been seen before in AA[52] and CG[53] simulations. The sugar rings of the different glycolipid headgroups are positioned at a very similar position along the bilayer normal for both thylakoid membranes. Even the two sugar rings of DGDG show strongly overlapping distributions, pointing to an overall perpendicular orientation of the ring–ring vector with respect to the membrane normal. This is also visible in the

snapshots (Fig. 6). A slight shift of the second sugar ring (GA) toward the aqueous solution is, however, noticeable. Interestingly, the PG headgroups are located most to the exterior of the bilayer in both the cyanobacterial and plant membrane.

In comparison to the atomistic data, the profiles show clearly that the CG membranes are somewhat thicker than the AA ones, as discussed above (cf. Table 4). In line with the larger area of the AA membranes, it appears that there is more water penetration in the atomistic membranes than in the CG membranes. Noticeable is also the somewhat smaller spread of the headgroups in the atomistic membranes in case of the plant membrane.

Another interesting observation is the closer approach of sodium to the membrane compared to chloride ions. This is seen at both AA and CG resolution and likely results from the electrostatic attraction between the negatively charged PG and SQDG lipids and the positive sodium ions. A similar condensation effect of counter ions has been reported in other atomistic simulations of anionic lipids [54]. Comparison of the hydration level of each lipid with its percentage of ion contacts (Table 6) demonstrates that the PG and SQDG headgroups indeed make relatively more contact with Na^+ compared to neutral headgroups. Another significant observation is the increased exposure to the solvent of DGDG compared to MGDG. This can be attributed to the large head group size of DGDG; in particular the second sugar ring is shifted toward the outer rim of the bilayer, and is therefore more solvent accessible (cf. Fig. 5).

Together, our analyses of the cross-sectional organization of the thylakoid membranes reveal a complex membrane/water interface, with all glycolipid sugar rings as well as PG head groups competing for the same space. The negatively charged PG and SQDG lipids attract counterions in their vicinity, leading to the formation of an electrical double layer. Overall, the plant membrane appears more diffuse compared to

Table 6

Lipid solvation properties. Contact percentages are shown between the lipid headgroups and water and sodium beads, respectively, based on the CG systems. Numbers indicate the percentage of the headgroup – water/sodium contacts compared with all headgroup – sodium/water contacts. Percentages between parentheses following the lipid names indicate the total share of that lipid in the system. Deviations in contact percentages of more than 20% from what can be expected from random solvation are shown in bold face. Cyanobacterial contact percentages are from the simulation at 293 K; the differences between those with the contact percentages of the simulation at 328 K are only minor. The standard error for the CG simulations is below 0.1%. For the calculation of the standard error it was assumed that every 250 ns of each leaflet counts as an independent observation.

	Water	Na$^+$
Cyanobacterial membrane		
18:1(9)-16:0 PG (10%)	8%	12%
18:1(9)-16:0 DGDG (25%)	**37%**	27%
18:1(9)-16:0 MGDG (40%)	29%	**26%**
18:1(9)-16:0 SQDG (10%)	10%	**14%**
di16:0 SQDG (15%)	15%	**21%**
Plant membrane		
16:1(3t)-16:0 PG (5%)	4%	**9%**
16:1(3t)-18:3(9,12,15) PG (10%)	9%	**15%**
18:3(9,12,15)-16:0 DGDG (5%)	**7%**	6%
di18:3(9,12,15) DGDG (25%)	**37%**	22%
18:3(9,12,15)-16:0 MGDG (5%)	**3%**	4%
di18:3(9,12,15) MGDG (40%)	**25%**	**19%**
18:3(9,12,15)-16:0 SQDG (15%)	15%	**25%**

the cyanobacterial membrane in the way the lipid moieties are distributed along the membrane normal.

3.4. Inverted hexagonal phase of the thylakoid membranes

To study the ability of the thylakoid membranes to form inverted hexagonal phases, we investigated the propensity for stalk formation as a function of hydration level. The stalk is the main intermediate in the transition from a lamellar phase to an inverted hexagonal phase [55,56]. A stalk can be formed when the headgroups of two apposed bilayers get into contact and start interacting, triggering the flipping of tails between the leaflets [57]. This depends on the amount of solvent

present between the two bilayers and the propensity of the bilayer to undulate. The more solvent present and the smaller the undulations of the membrane, the less likely the bilayers make contact and form a stalk. By varying the hydration level in simulations involving a double bilayer setup, we probed the propensity of stalk formation (see Methods). Fig. 7 shows snapshots from the process of stalk formation in both the cyanobacterial (at T = 328 K) and plant membrane (T = 293 K). In case of the cyanobacterial membrane, a spontaneous stalk can only be triggered at hydration levels of 6 CG water beads per lipid (equivalent to 24 AA water molecules per lipid) and below. The plant membrane, which exhibits more pronounced undulations, forms a spontaneous stalk already at a hydration level of 9 CG waters per lipid (36 AA waters per lipid). In each case, after the stalk has formed, the stalk elongates until it connects with its periodic boundary image, thereby transforming the lamellar state into the inverted hexagonal one. The lamellar to inverted hexagonal transformation of the thylakoid membrane is similar to the transformation described for unsaturated PC lipids [58], also based on CG simulations.

To pinpoint the critical hydration level for the lamellar to inverted hexagonal phase transformation more precisely, we performed a systematic set of simulations in which we started from a state in which a stalk had already formed. If the stalk started growing, we increased the hydration level, until we reached a point where the stalk no longer elongated. Vice versa, if the stalk disappeared, we lowered the hydration level until the stalk proved stable. For the cyanobacterial membrane at 293 K, we found that 7.3 CG water beads per lipid (29.2 AA waters per lipid) are needed to stabilize the stalk. At 328 K, the hydration level needed to be increased to 9.0 CG water beads per lipid (36 AA waters per lipid). For the plant membrane, a further increase to 12.5 CG water beads per lipid (50 AA waters per lipid) was required to stabilize the stalk. These results confirm that the plant membrane has a higher propensity to form an inverted hexagonal phase compared to the cyanobacterial membrane. We attribute this difference to the presence of polyunsaturated fatty acids in the plant membrane. Polyunsaturated lipids have a large negative spontaneous curvature, which stabilizes the stalk state. Moreover, the increased flexibility and less hydrophobic nature of polyunsaturated chains compared to fully saturated
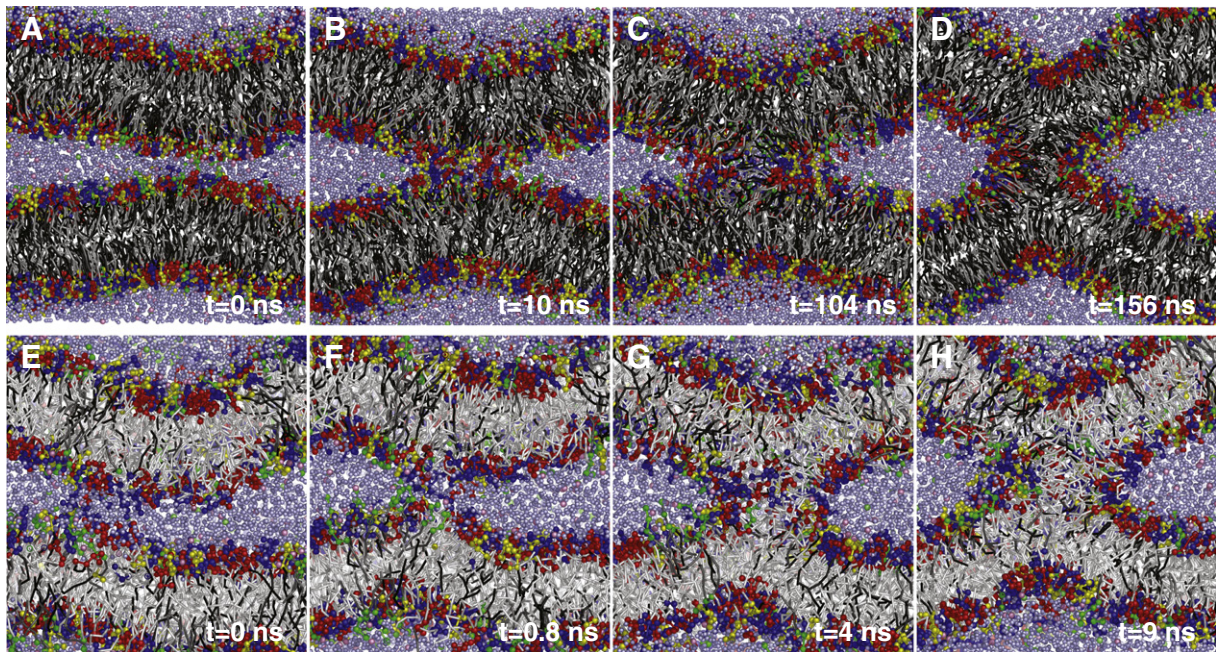
Fig. 7. Stalk formation in thylakoid membrane stacks. Snapshots of the spontaneous stalk formation between two leaflets of the CG cyanobacterial membrane at 328 K and hydration level of 5 CG water beads per lipid (equivalent to 20 AA water molecules per lipid) (A–D) and the CG plant membrane at 293 K and hydration level of 9 CG water beads per lipid (36 AA waters per lipid) (F–H).

chains increases their exposure at the lipid/water interface by means of back-folding. Solvent-exposed tails in general, and polyunsaturated lipids in particular, are key intermediates in the formation of a stalk at the onset of membrane fusion and fission [57,59,60].

Our simulations demonstrate that the thylakoid membrane is close to the formation of an inverted hexagonal phase. Inverted hexagonal phases have been shown to be present in thylakoids [11] and it has been established experimentally that their formation depends on temperature [11], fatty acid saturation grade [61] and hydration level [62], which is in line with our data. Inverted hexagonal phases might be vital in regulating photosynthesis by tuning the activity of the violaxanthin cycle [13,63].

We did not observe the formation of any MGDG clusters in the inverted hexagonal phase, as was proposed in the literature [12,13]. Instead, we see a well mixed system in both the lamellar and inverted hexagonal state, as was seen experimentally on the mesoscopic scale [16].

3.5. Conformation and dynamics of the plastoquinone pool

The organization and dynamics of the cofactors plastoquinone (PL9one) and plastoquionol (PL9ol) in the thylakoid membrane, the so-called plastoquinone-pool, is of great importance for the transport of protons to the lumen and of electrons between different protein complexes in the photosynthetic pathway. We simulated PL9one and PL9ol in the cyanobacterial thylakoid membrane, at T = 310 K and at a molar concentration of about 0.5%. Representative snapshots of the simulation in case of PL9one are shown in Fig. 8. The cofactors can be seen to reside with their head groups at the level of the glycerol linker, with the aliphatic tails pointing inside. The embedding of PL9ol is rather similar (not shown).

Cluster analysis of the molecular conformations showed three preferred orientations of the cofactors, the L-, the I- and the U-conformation that differ in the position and shape of the tail. In the L-conformation the PL9one tail is in a L-shape, where the vertical part of the 'L' extends from the headgroup region of one leaflet towards the bilayer midplane and the horizontal part of the 'L' proceeds into the midplane of the bilayer (Fig. 8A). In the I-conformation the tail extends from the headgroup region of one leaflet into the opposite monolayer, sometimes with slight S-turn at the bilayer midplane (Fig. 8B). In the U-conformation the tail curls back up to the head group region of the same leaflet (Fig. 8C). The ratios of L, I and U conformations were 58(1):14(3):15(4)% and 61(1):10(3):17(2)% for the systems containing PL9ones and PL9ols, respectively. The values between parentheses indicate the standard deviation calculated over the four solutes. The PL9ones and PL9ols adapted, respectively, 87% and 88% percent of the time a L, I or U conformation, The remaining 13% and 12% consist of less well defined, often less extended, conformations. The dominant conformation, both for PL9one and PL9ol, is the L-shape. A similar conclusion was reached from CG simulations of these cofactors in a DPPC membrane, using a similar setup [37].

During the 3 μs simulation, the PL9one head group was observed to flip from one monolayer to the other, a so-called flip-flop event. In total, eighteen flip-flop events were counted for the four PL9one molecules present, resulting in a flip-flop rate of 1.5×10^6 s^{-1}. This rate is about one order of magnitude slower compared to the flip-flop rate in a DPPC bilayer [37]. For the 3.5 μs simulation containing PL9ol no flip-flop events were observed, whereas a flip-flop rate of 5×10^5 s^{-1} was reported for the DPPC membrane. The much lower flip-flop rate of PL9ol as compared to PL9one is due to the more hydrophilic head group of PL9ol. The lower flip-flop rates in the cyanobacterial thylakoid membrane compared to a DPPC membrane can be attributed to the more compact nature of the former.

Summarizing, our simulations of PL9one and PL9ol showed that these cofactors can adapt different conformations in the thylakoid
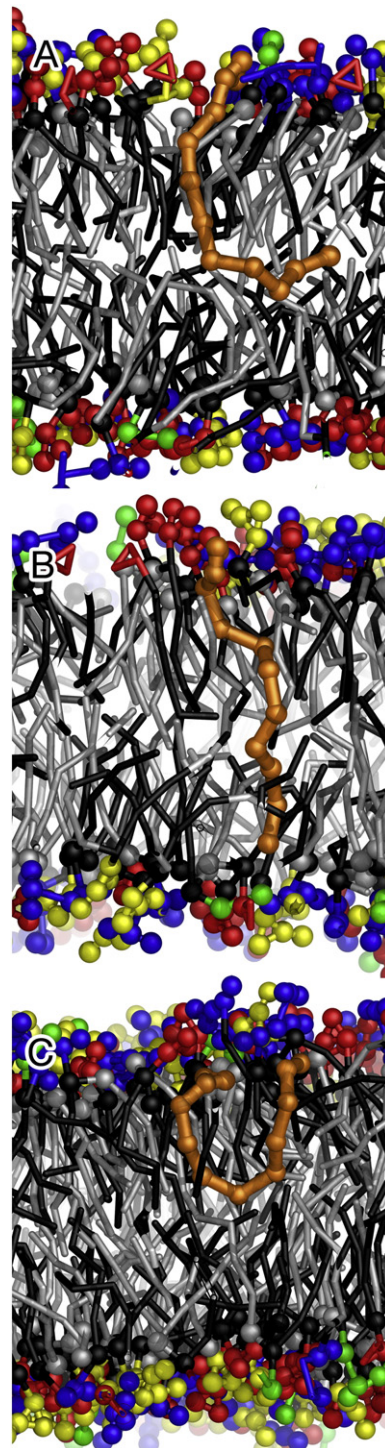
Fig. 8. Conformations of plastoquinone in the cyanobacterial thylakoid membrane. Snapshots of plastoquinone in the L (A), I (B) and U (C) conformation.

membrane and that the more hydrophilic PL9ol makes fewer flip-flops.

4. Conclusion

Using a multiscale approach, we modeled the thylakoid membranes of two different species, namely cyanobacteria and higher plants. Contact analysis, as well as visual inspection, reveals that the lipids in both membranes are distributed homogeneously on the microscopic scale. Not all lipids mix ideally however, and heterogeneities on the

nanoscale occur. For instance negative charged lipids have a tendency to repel each other, and DGDG lipids avoid self-interaction probably due to steric hindrance of the bulky headgroups. In the more complex plant membrane the mixing is not only determined by the headgroups, but also by the lipid tails. In particular, lipids with fully saturated fatty acids tend to cluster.

Due to the presence of more saturated lipid tails, the cyanobacterial membrane is thicker, denser, more ordered and less compressible compared to the plant membrane. Even at the elevated temperature of 328 K, the cyanobacterial remains less fluid than the plant membrane at room temperature. The integrity of the cyanobacterial membrane is likely important considering the harsh conditions under which cyanobacteria operate. Electron densities of both thylakoid membranes demonstrate a similar transmembrane organization, with the sugar rings of the glycolipids occupying overlapping positions at the membrane/water interface. The PG headgroups are located more to the exterior of the bilayer. In line with the more fluid character of the plant membrane, the electron density distributions have a bigger spread than those of the cyanobacterial membrane. We find that the plant membrane also has a higher propensity to form an inverted hexagonal phase. Whether this difference is physiologically important, however, remains unclear.

Our characterization of the molecular structure of the thylakoid membrane opens the way for future studies involving the embedded photosynthetic complexes. For instance, it will be interesting to see whether specific lipid binding sites exist, similar to the membrane exposed cardiolipin binding sites recently revealed on mitochondrial respiratory chain complexes [64–66]. Understanding the interplay between the specific lipids found in the thylakoid membrane and the formation of photosystem supercomplexes is an open problem, ready to be explored using multiscale simulations.

Transparency Document

The Transparency document associated with this article can be found, in the online version.

Acknowledgements

References

[1] R.E. Blankenship, Molecular mechanisms of photosynthesis, Blackwell Science, 2002.
[2] P.A. Siegenthaler, N. Murata, Lipids in Photosynthesis: Structure, Function, and Genetics, Kluwer Academic Publishers London, UK, 1998.
[3] I. Sakurai, J. Shen, J. Leng, S. Ohashi, M. Kobayashi, H. Wada, Lipids in oxygen-evolving photosystem II complexes of cyanobacteria and higher plants, J. Biochem. 140 (2) (2006) 201–209.
[4] N. Murata, I. Nishida, Lipids of blue-green algae (cyanobacteria), Biochem. plants compr. treatise 9 (1987).
[5] L. Boudière, M. Michaud, D. Petroutsos, F. Rébeillé, D. Falconet, O. Bastien, S. Roy, G. Finazzi, N. Rolland, J. Jouhet, Glycerolipids in photosynthesis: composition, synthesis and trafficking, Biochim. Biophys. Acta Bioenerg. 1837 (4) (2014) 470–480.
[6] W.P. Williams, The physical properties of thylakoid membrane lipids and their relation to photosynthesis, Lipids in Photosynthesis: Structure, Function and Genetics, Springer, Dordrecht, 2004, pp. 103–118.
[7] W. Williams, P. Quinn, The phase behavior of lipids in photosynthetic membranes, J. Bioenerg. Biomembr. 19 (6) (1987) 605–624.
[8] K. Gounaris, A. Sen, A.P. Brain, P.J. Quinn, W. Patrick Williams, The formation of non-bilayer structures in total polar lipid extracts of chloroplast membranes, Biochim. Biophys. Acta Biomembr. 728 (1) (1983) 129–139.
[9] G. Graham Shipley, J.P. Green, B.W. Nichols, The phase behavior of monogalactosyl, digalactosyl, and sulphoquinovosyl diglycerides, Biochim. Biophys. Acta Biomembr. 311 (4) (1973) 531–544.
[10] C.P.S. Tilcock, Lipid polymorphism, Chem. Phys. Lipids 40 (2–4) (1986) 109–125.
[11] S.B. Krumova, C. Dijkema, P. de Waard, H. Van As, G. Garab, H. van Amerongen, Phase behavior of phosphatidylglycerol in spinach thylakoid membranes as revealed by ^{31}P-NMR, Biochimic. Biophys. Acta Biomembr. 1778 (4) (2008) 997–1003.

[12] R. Goss, D. Latowski, J. Grzyb, A. Vieler, M. Lohr, C. Wilhelm, K. Strzalka, Lipid dependence of diadinoxanthin solubilization and de-epoxidation in artificial membrane systems resembling the lipid composition of the natural thylakoid membrane, Biochim. Biophys. Acta Biomembr. 1768 (1) (2007) 67–75.
[13] P. Jahns, D. Latowski, K. Strzalka, Mechanism and regulation of the violaxanthin cycle: the role of antenna proteins and membrane lipids, Biochim. Biophys. Acta 1787 (1) (2009) 3–14.
[14] S. Schaller, D. Latowski, M. Jemioła-Rzemińska, C. Wilhelm, K. Strzałka, R. Goss, The main thylakoid membrane lipid monogalactosyldiacylglycerol (MGDG) promotes the de-epoxidation of violaxanthin associated with the light-harvesting complex of photosystem II (LHCII), Biochim. Biophys. Acta 1797 (3) (2010) 414–424.
[15] P. Siegenthaler, Molecular organization of acyl lipids in photosynthetic membranes of higher plants, Lipids in Photosynthesis: Structure, Function and Genetics, Kluwer Academic Publishers, Dordrecht, The Netherlands, 1998, pp. 119–144.
[16] S. Duchêne, P. Siegenthaler, Do glycerolipids display lateral heterogeneity in the thylakoid membrane? Lipids 35 (7) (2000) 739–744.
[17] S.J. Marrink, A.H. de Vries, D.P. Tieleman, Lipids on the move: simulations of membrane pores, domains, stalks and curves, Biochim. Biophys. Acta Biomembr. 1788 (1) (2009) 149–168.
[18] I. Vattulainen, T. Rog, Lipid simulations: a perspective on lipids in action, Cold Spring Harb. Perspect. Biol. 3 (4) (2011).
[19] M. Manna, T. Rog, I. Vattulainen, The challenges of understanding glycolipid functions: an open outlook based on molecular simulations, Biochimica et Biophysica Acta (BBA) - Molecular and Cell Biology of Lipids 1841 (2014) 1130–1145.
[20] J. Kapla, B. Stevensson, M. Dahlberg, A. Maliniak, Molecular dynamics simulations of membranes composed of glycolipids and phospholipids, J. Phys. Chem. B 116 (1) (2011) 244–252.
[21] S. Vasil'ev, D. Bruce, A protein dynamics study of photosystem II: the effects of protein conformation on reaction center function, Biophys. J. 90 (9) (2006) 3062–3073.
[22] K. Ogata, T. Yuki, M. Hatakeyama, W. Uchida, S. Nakamura, All-atom molecular dynamics simulation of photosystem ii embedded in thylakoid membrane, J. Am. Chem. Soc. 135 (42) (2013) 15670–15673.
[23] K. Onai, M. Morishita, S. Itoh, K. Okamoto, M. Ishiura, Circadian rhythms in the thermophilic cyanobacterium Thermosynechococcus elongatus: compensation of period length over a wide temperature range, J. Bacteriol. 186 (15) (2004) 4972–4977.
[24] S. Albers, J. Van de Vossenberg, A. Driessen, W.N. Konings, Adaptations of the archaeal cell membrane to heat stress, Front. Biosci. 5 (2000) D813–D820.
[25] N. Russell, N. Fukunaga, A comparison of thermal adaptation of membrane lipids in psychrophilic and thermophilic bacteria, FEMS Microbiol. Lett. 75 (2-3) (1990) 171–182.
[26] J. Reizer, N. Grossowicz, Y. Barenholz, The effect of growth temperature on the thermotropic behavior of the membranes of a thermophilic *Bacillus*, Biochim. Biophys. Acta Biomembr. 815 (2) (1985) 268–280.
[27] S.J. Marrink, D.P. Tieleman, Perspective on the Martini model, Chem. Soc. Rev. 42 (2013) 6801–6822.
[28] S.J. Marrink, H.J. Risselada, S. Yefimov, D.P. Tieleman, A.H. de Vries, The MARTINI force field: coarse grained model for biomolecular simulations, J. phys. Chem. B 111 (27) (2007) 7812–7824.
[29] N. Murata, H. Wada, Z. Gombos, Modes of fatty-acid desaturation in cyanobacteria, Plant Cell Physiol. 33 (7) (1992) 933–941.
[30] Y.L. Ya'Acov, Membrane fatty acyl tailgroups, Plant Membranes, Springer, Dordrecht, 1992, pp. 11–26.
[31] J. Browse, P.J. McCourt, C.R. Somerville, Fatty acid composition of leaf lipids determined after combined digestion and fatty acid methyl ester formation from fresh tissue, Anal. Biochem. 152 (1) (1986) 141–145.
[32] J.G. Wallis, J. Browse, Mutants of *Arabidopsis* reveal many roles for membrane lipids, Prog. Lipid Res. 41 (3) (2002) 254–278.
[33] M. Bulacu, X. Periole, S.J. Marrink, In silico design of robust bolalipid membranes, Biomacromolecules 13 (1) (2011) 196–205.
[34] N. Kučerka, J. Gallová, D. Uhríková, P. Balgavý, M. Bulacu, S. Marrink, J. Katsaras, Areas of monounsaturated diacylphosphatidylcholines, Biophys. J. 97 (7) (2009) 1926–1932.
[35] H.I. Ingólfsson, M.N. Melo, F.J. van Eerden, C. Arnarez, C.A. Lopez, T.A. Wassenaar, X. Periole, A.H. De Vries, D.P. Tieleman, S.J. Marrink, Lipid organization of the plasma membrane, J. Am. Chem. Soc. 136 (41) (2014) 14554–14559.
[36] C.A. López, Z. Sovova, F.J. van Eerden, A.H. de Vries, S.J. Marrink, Martini force field parameters for glycolipids, J. Chem. Theory Comput. 9 (3) (2013) 1694–1708.
[37] D.H. de Jong, N. Liguori, T. van der Berg, C. Arnarez, X. Periole, S.J. Marrink, Parameterization of thylakoid cofactors at atomistic and coarse grain resolution, J. Phys. Chem. B (2015) (submitted for publication).
[38] B. Hess, C. Kutzner, D. van der Spoel, E. Lindahl, GROMACS 4: algorithms for highly efficient, load-balanced, and scalable molecular simulation, J. Chem. Theory Comput. 4 (3) (2008) 435–447.
[39] T.A. Wassenaar, H.I. Ingólfsson, R.A. Böckmann, D.P. Tieleman, S.J. Marrink, Computational lipidomics with insane: a versatile tool for generating custom membranes for molecular simulations, J. Chem. Theory Comput. (2015) (in press).
[40] H.J. Berendsen, J.P.M. Postma, W.F. van Gunsteren, A. DiNola, J. Haak, Molecular dynamics with coupling to an external bath, J. Chem. Phys. 81 (1984) 3684.
[41] S. Ramadurai, A. Holt, L.V. Schäfer, V.V. Krasnikov, D.T. Rijkers, S.J. Marrink, J.A. Killian, B. Poolman, Influence of hydrophobic mismatch and amino acid composition on the lateral diffusion of transmembrane peptides, Biophys. J. 99 (5) (2010) 1447–1454.
[42] M. Fuhrmans, V. Knecht, S.J. Marrink, A single bicontinuous cubic phase induced by fusion peptides, J. Am. Chem. Soc. 131 (26) (2009) 9166–9167.

[43] A.J. Rzepiela, L.V. Schäfer, N. Goga, H.J. Risselada, A.H. De Vries, S.J. Marrink, Reconstruction of atomistic details from coarse-grained structures, J. Comput. Chem. 31 (6) (2010) 1333–1343.

[44] C. Oostenbrink, A. Villa, A.E. Mark, W.F. van Gunsteren, A biomolecular force field based on the free enthalpy of hydration and solvation: the GROMOSforce-fieldparameter sets 53A5 and 53A6, J. Comput. Chem. 25 (13) (2004) 1656–1676.

[45] T. Darden, D. York, L. Pedersen, Particle mesh Ewald: an $N \cdot \log (N)$ method for Ewald sums in large systems, J. Chem. Phys. 98 (1993) 10089.

[46] U. Essmann, L. Perera, M.L. Berkowitz, T. Darden, H. Lee, L.G. Pedersen, A smooth particle mesh Ewald method, J. Chem. Phys. 103 (19) (1995) 8577–8593.

[47] S.E. Feller, R.W. Pastor, Constant surface tension simulations of lipid bilayers: the sensitivity of surface areas and compressibilities, J. Chem. Phys. 111 (3) (1999) 1281.

[48] X. Daura, K. Gademann, B. Jaun, D. Seebach, W.F. van Gunsteren, A.E. Mark, Peptide folding: when simulation meets experiment, Angew. Chem. Int. Ed. 38 (1-2) (1999) 236–240.

[49] M. Sarcina, N. Murata, M.J. Tobin, C.W. Mullineaux, Lipid diffusion in the thylakoid membranes of the cyanobacterium Synechococcus sp.: effect of fatty acid desaturation, FEBS Lett. 553 (3) (2003) 295–298.

[50] A. Hall, T. Róg, I. Vattulainen, Effect of galactosylceramide on the dynamics of cholesterol-rich lipid membranes, J. Phys. Chem. B 115 (49) (2011) 14424–14434.

[51] A. Filippov, G. Orädd, G. Lindblom, The effect of cholesterol on the lateral diffusion of phospholipids in oriented bilayers, Biophys. J. 84 (5) (2003) 3079–3086.

[52] S.E. Feller, K. Gawrisch, A.D. MacKerell, Polyunsaturated fatty acids in lipid bilayers: intrinsic and environmental contributions to their unique physical properties, J. Am. Chem. Soc. 124 (2) (2002) 318–326.

[53] H.J. Risselada, S.J. Marrink, Curvature effects on lipid packing and dynamics in liposomes revealed by coarse grained molecular dynamics simulations, Phys. Chem. Chem. Phys. 11 (12) (2009) 2056–2067.

[54] S.A. Pandit, D. Bostick, M.L. Berkowitz, Molecular dynamics simulation of a dipalmitoylphosphatidylcholine bilayer with NaCl, Biophys. J. 84 (6) (2003) 3743–3750.

[55] M. Kozlov, S. Leikin, L. Chernomordik, V. Markin, Y.A. Chizmadzhev, Stalk mechanism of vesicle fusion, Eur. Biophys. J. 17 (3) (1989) 121–129.

[56] D. Siegel, R. Epand, The mechanism of lamellar-to-inverted hexagonal phase transitions in phosphatidylethanolamine: implications for membrane fusion mechanisms, Biophys. J. 73 (6) (1997) 3089–3111.

[57] Y.G. Smirnova, S. Marrink, R. Lipowsky, V. Knecht, Solvent-exposed tails as prestalk transition states for membrane fusion at low hydration, J. Am. Chem. Soc. 132 (19) (2010) 6710–6718.

[58] S. Marrink, A.E. Mark, Molecular view of hexagonal phase formation in phospholipid membranes, Biophys. J. 87 (6) (2004) 3894–3900.

[59] A.J. Markvoort, S.J. Marrink, Lipid acrobatics in the membrane fusion arena, Curr. Top. Membr. 68 (2011) 259–294.

[60] M. Pinot, S. Vanni, S. Pagnotta, S. Lacas-Gervais, L.A. Payet, T. Ferreira, R. Gautier, B. Goud, B. Antonny, H. Barelli, Polyunsaturated phospholipids facilitate membrane deformation and fission by endocytic proteins, Science 345 (6197) (2014) 693–697.

[61] R.N. Lewis, D.A. Mannock, R.N. McElhaney, D.C. Turner, S.M. Gruner, Effect of fatty acyl chain length and structure on the lamellar gel to liquid-crystalline and lamellar to reversed hexagonal phase transitions of aqueous phosphatidylethanolamine dispersions, Biochemistry 28 (2) (1989) 541–548.

[62] B. Deme, C. Cataye, M.A. Block, E. Marechal, J. Jouhet, Contribution of galactoglycerolipids to the 3-dimensional architecture of thylakoids, FASEB J. Off. Publ. Fed. Am. Soc. Exp. Biol. 28 (8) (2014) 3373–3383.

[63] D. Latowski, J. Kruk, K. Burda, M. Skrzynecka-Jaskier, A. Kostecka-Gugała, K. Strzałka, Kinetics of violaxanthin de-epoxidation by violaxanthin de-epoxidase, a xanthophyll cycle enzyme, is regulated by membrane fluidity in model lipid bilayers, Eur. J. Biochem. 269 (18) (2002) 4656–4665.

[64] C. Arnarez, S. Marrink, X. Periole, Identification of cardiolipin binding sites on cytochrome c oxidase at the entrance of proton channels, Sci. Rep. 3 (2013).

[65] C. Arnarez, J. Mazat, J. Elezgaray, S. Marrink, X. Periole, Evidence for cardiolipin binding sites on the membrane-exposed surface of the cytochrome bc 1, J. Am. Chem. Soc. 135 (8) (2013) 3112–3120.

[66] S. Pöyry, O. Cramariuc, P.A. Postila, K. Kaszuba, M. Sarewicz, A. Osyczka, I. Vattulainen, T. Róg, Atomistic simulations indicate cardiolipin to have an integral role in the structure of the cytochrome bc_1 complex, Biochim. Biophys. Acta Bioenerg. 1827 (6) (2013) 769–778.